Cell Reports, Volume *42*

Supplemental information

Peptidergic and functional delineation of the Edinger-Westphal nucleus

Michael F. Priest, Sara N. Freda, Isabelle J. Rieth, Deanna Badong, Vasin Dumrongprechachan, and Yevgenia Kozorovitskiy

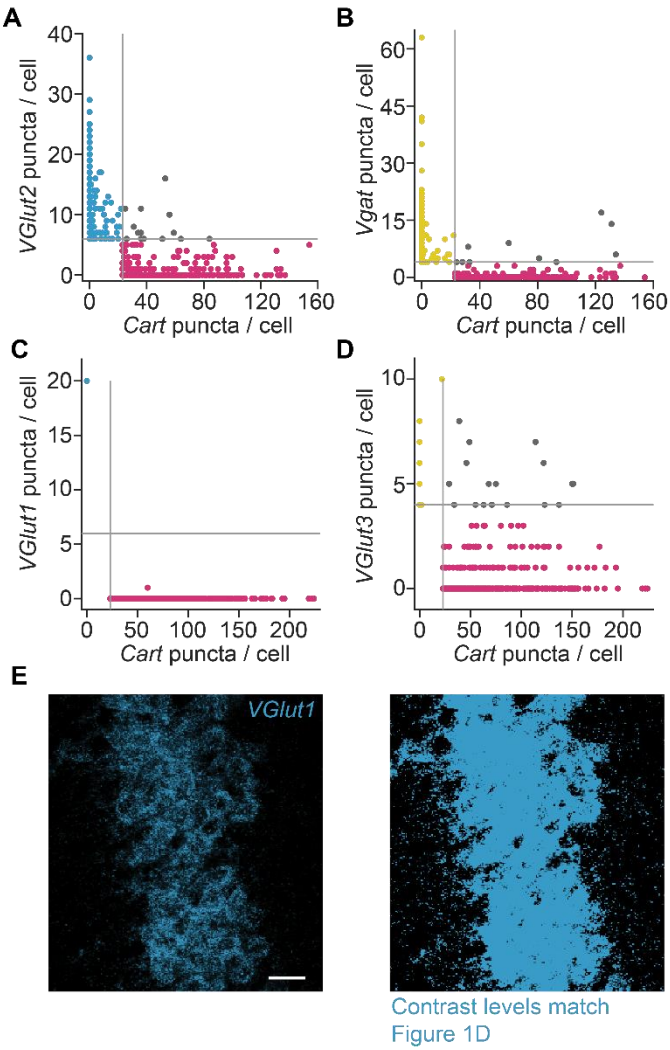

Figure S1. Quantification of vesicular transporter transcripts. Related to Figure 1.

(A) Quantification of puncta per cell in the EW and peri-EW regions for *VGlut2*/*Slc17a6* (blue, 744 neurons), and *Cart*/*Cartpt* (red, 297 neurons). Gray lines denote thresholds above which neurons were considered positive for the transcript, and gray dots are neurons positive for both transcripts (15 neurons). Data are pooled from 3 mice here and in (B-D).

(B) As in (A) but for *Vgat*/*Slc32a1* (yellow, 249 neurons). 10 neurons are positive for both.

(C) Similar to (A), but for *VGlut1*/*Slc17a7* (blue, 1 neuron) against *Cart* neurons (red, 404 neurons). 0 neurons are positive for both.

(D) As in (C), but for *VGlut3*/*Slc17a8* (yellow, 28 neurons). 17 neurons are positive for both.

(E) Robust *VGlut1* transcript signal is seen in the hippocampus (left; scale, 20 µm). The same image is shown on the right, with contrast levels set identical to those used in the main text for *VGlut1*. Absence of *VGlut1*/*Slc17a7*-positive neurons in and near the EW is not due to insufficient probe labeling.

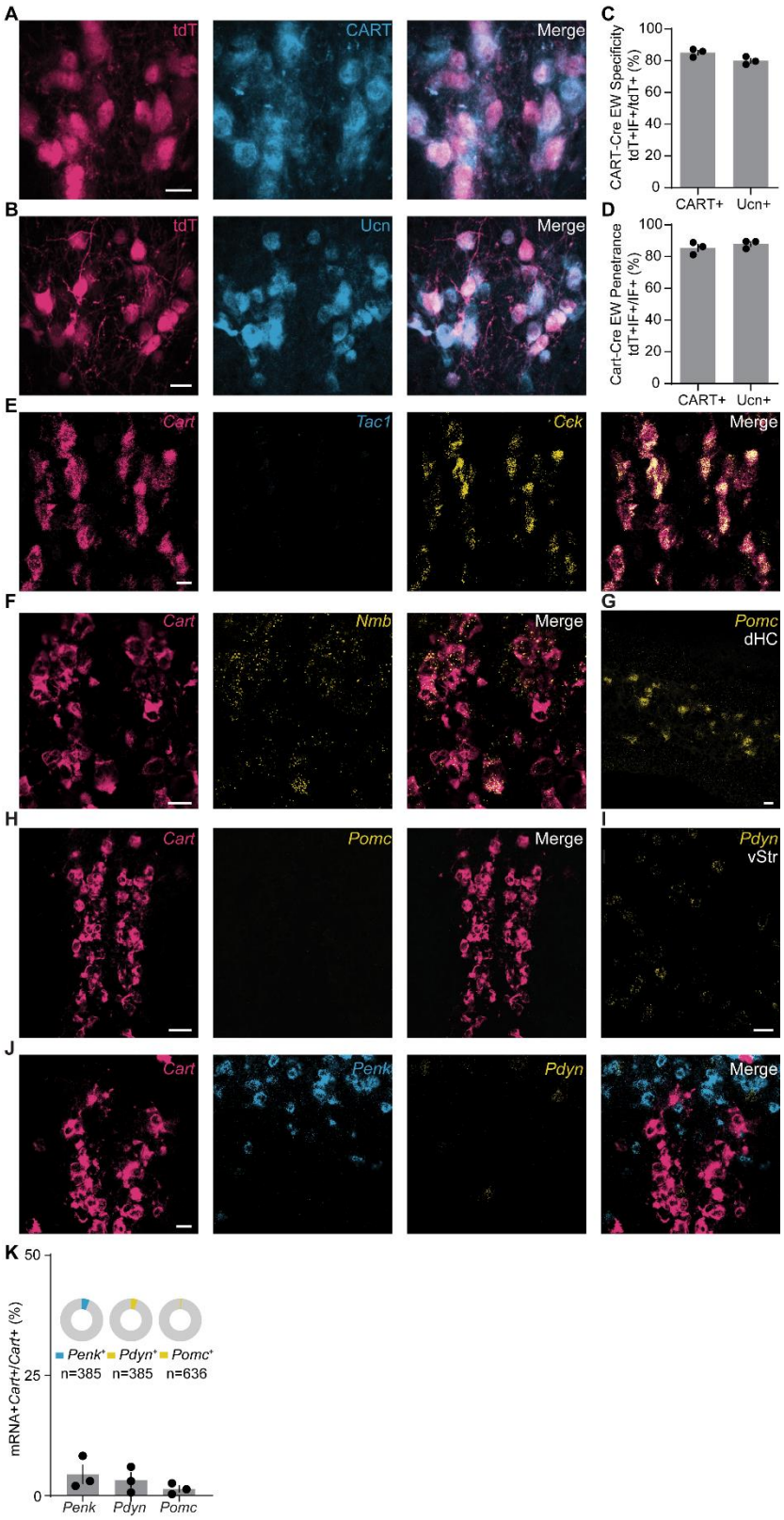

Figure S2. Genetic targeting and neuropeptides of the CART⁺ EW. Related to Figure 2.
(A) tdT⁺ neurons of the EW (left, red) compared to immunofluorescence against CART peptide (middle, blue) show high levels of colocalization (right, merge, magenta). Scale, 20 µm.

(B) As in (A) but with immunofluorescence against urocortin (blue).
(C) Quantification of tdT^+ EW cells positive for CART (85.1%±1.5%, n=3 mice, 784 cells) and urocortin (Ucn, 80.0%±1.4%, n=3 mice, 631 cells).
(D) Quantification of $CART^+$ (85.5%±2.3%, n=3 mice, 677 cells) and Ucn^+ (88.0%±1.5%, n=3 mice, 574 cells) that are tdT^+.
(E) FISH against *Cart* (red), *Tac1*/*Sub. P* (blue) and *Cck* (yellow). As seen in the merge, there is robust colocalization between *Cck* and *Cart*. Scale, 20 µm.
(F) Similar to (E), but *Cart* (red) and *Nmb* (yellow) showing colocalization in some EW neurons (merge).
(G) Absence of *Pomc* neurons in and near the EW is not due to poor probe labeling. FISH against *Pomc* (yellow) shows clear signal in the dorsal hippocampus. Scale, 20 µm.
(H) FISH of the EW region against *Cart* (red) and *Pomc* (yellow) shows no colocalization in $CART^+$ EW neurons (merge). Scale, 20 µm.
(I) As in (G), but against *Pdyn* in the ventral striatum. Scale, 20 µm.
(J) As in (H), but against *Penk* (blue), and *Pdyn* (yellow).
(K) EW *Cart* does not colocalize with opioid-encoding mRNAs (*Penk*, 4.44% ± 1.93%; *Pdyn*, 3.22% ± 1.55%, *Pomc*, 1.40% ± 0.65%, n = 3 mice, inset pie graphs show pooled $Cart^+$ count). Error bars represent SEM.

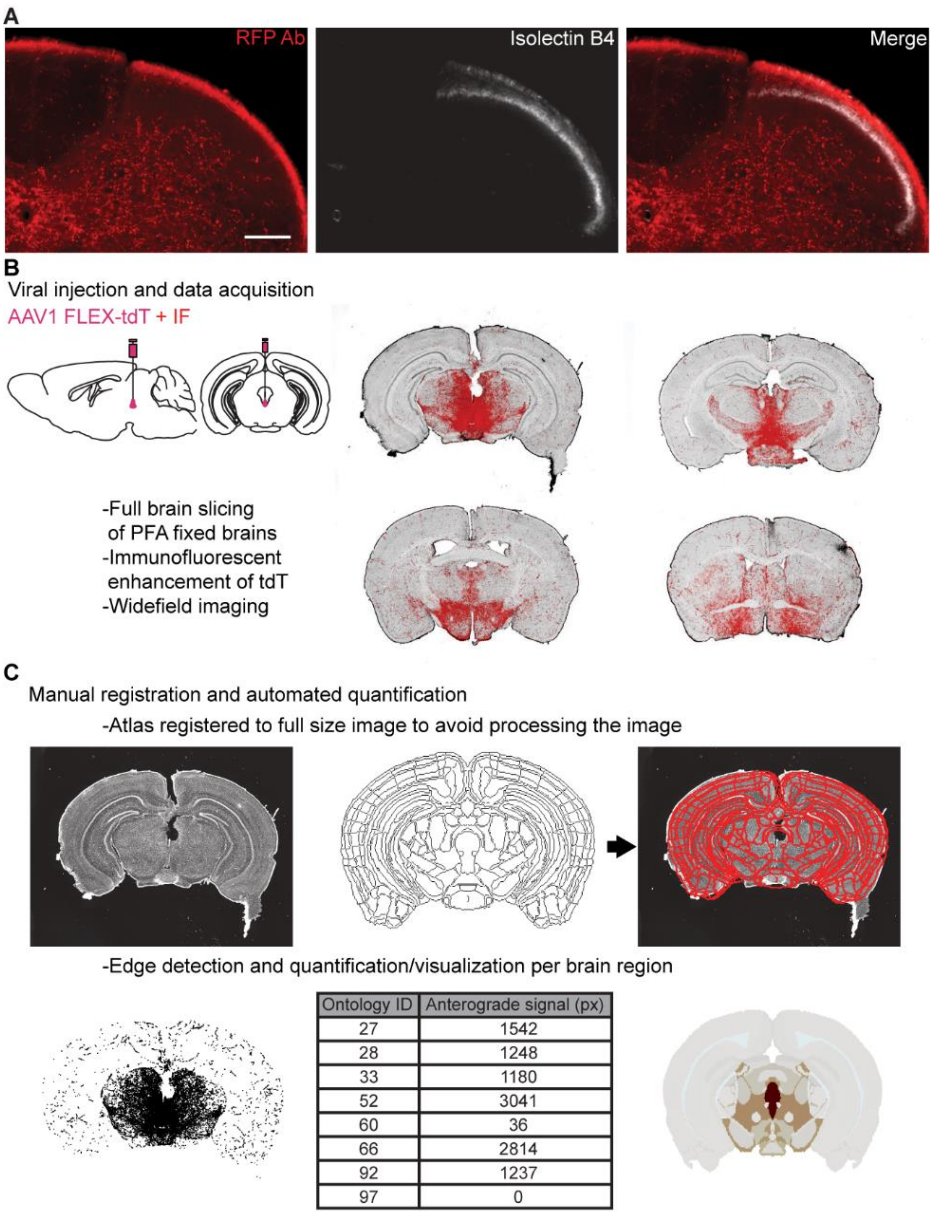

Ontology ID	Anterograde signal (px)
27	1542
28	1248
33	1180
52	3041
60	36
66	2814
92	1237
97	0

Figure S3. Spinal cord lamina labeling and whole brain mapping of CART⁺ EW projections. Related to Figure 3.

(A) CART⁺ EW projections (red) in the spinal cord do not appear to extend to lamina II, marked with isolectin B4 (white), but are found in the pain- and mechanically-sensitive dorsal horn and lamina X. Scale, 100 µm.

(B) Visualization of the whole brain mapping pipeline. Injection of AAV FLEX-tdTomato in the CART⁺ EW was followed by fixed slicing, immunofluorescent enhancement of tdTomato, and widefield fluorescent imaging to produce whole brain sections (set of 4 is shown here as an example).

(C) Brain sections (top left) were manually registered to coronal slices from the Allen Brain Atlas (top, middle; registration overlay at top, right). Edge detection (bottom, left) was performed to find neuronal processes throughout the brain section. Processes were quantified for each brain region (bottom, middle) and visualized as a heatmap.

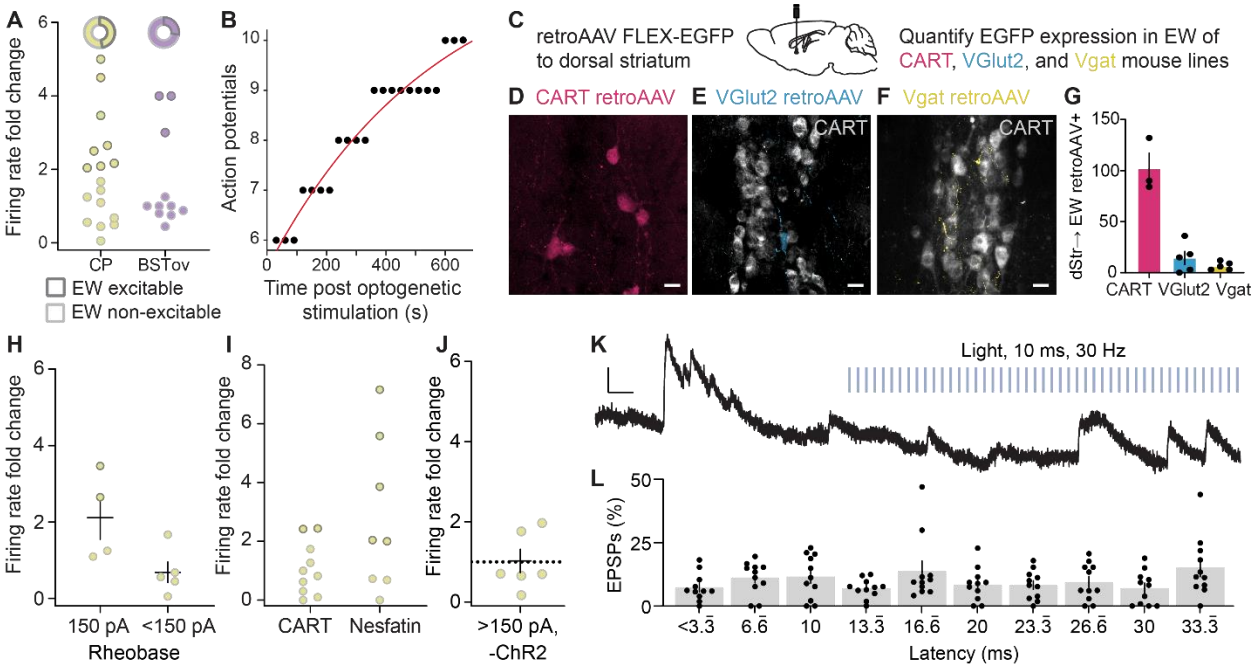

Figure S4. Functional peptidergic projections of the CART$^+$ EW. Related to Figure 4.

(A) Firing rate fold change of neurons recorded from CP (yellow) and BSTov (purple). Below, neurons in each region increase firing rate >2x following optical stimulation (dark gray, 8 of 17 SPNs in CP; 3 of 11 BSTov neurons; CP neurons from 11 mice, BSTov neurons from 7 mice).

(B) Time constants of the increase in firing rate of downstream neurons following optogenetic stimulation were calculated by taking an exponential fit (red line) of the number of action potentials over time following the beginning of optogenetic stimulation.

(C) Schematic of retroAAV FLEX-EGFP injection to the dorsal striatum of CART-Cre, VGlut2-Cre, and Vgat-Cre mice, followed by quantification of EGFP$^+$ neurons in the EW.

(D) Confocal image of FLEX-EGFP$^+$ neurons (red) in the EW of CART-Cre mice.

(E) Confocal image of FLEX-EGFP$^+$ neurons (blue) in the EW of VGlut2-Cre mice. CART peptide (gray) is used to define the EW. Few VGlut2-Cre$^+$ neurons are EGFP$^+$, and these neurons do not colocalize with CART.

(F) As in (E), but in the EW of a Vgat-Cre mouse.

(G) Summary of quantification of EGFP$^+$ neurons in the EW following retroAAV injection to the dorsal striatum. CART-Cre (red) = 102 ± 15.1 neurons, n = 3 mice; VGlut2-Cre (blue) = 14.4 ± 6.4 neurons, n = 5 mice; Vgat-Cre (yellow) = 6.6 ± 1.7 neurons; n = 5 mice.

(H) CP SPNs with rheobase equal to or less than 150 pA did not generally increase their firing rate. Rheobase = 150 pA: p = 0.1458, paired t-test, $t_{(3)}$ = 1.953, n = 4 neurons from 3 mice; rheobase <150 pA: p = 0.2978, paired t-test, $t_{(4)}$ = 1.196, n = 5 neurons from 5 mice.

(I) Application of CART to SPNs with a rheobase >150 pA did not produce increases in firing rate (2/10 neurons more than doubled their firing rate following CART application, p = 0.8070, paired t-test, $t_{(9)}$ = 0.2516, n = 10 neurons from 8 mice). However, application of nesfatin did (5/8 neurons more than doubled their firing rate following nesfatin application, p = 0.0930, paired t-test, $t_{(7)}$ = 1.944, n = 8 neurons from 5 mice).

(J) CP SPNs with rheobase >150 pA did not increase to light stimulation in the absence of $CART^+$ EW ChR2. p = 0.9367, paired t-test, $t_{(5)}$ = 0.0834, n = 6 neurons from 2 mice.
(K) Optogenetic stimulation did not elicit EPSPs in neurons activated by ChR2 $CART^+$ EW fibers. Blue lines denote light pulses. Scale, 0.5 mV, 100 ms.
(L) Quantification of EPSP latencies (ms) binned by 3.3 ms across the 33.33 ms interstimulus interval. No bin had a higher proportion of EPSPs than any other (p = 0.2923, repeated measures one-way ANOVA $F_{(2.575, 25.75)}$ = 1.307, n = 11 neurons).
Error bars represent SEM.

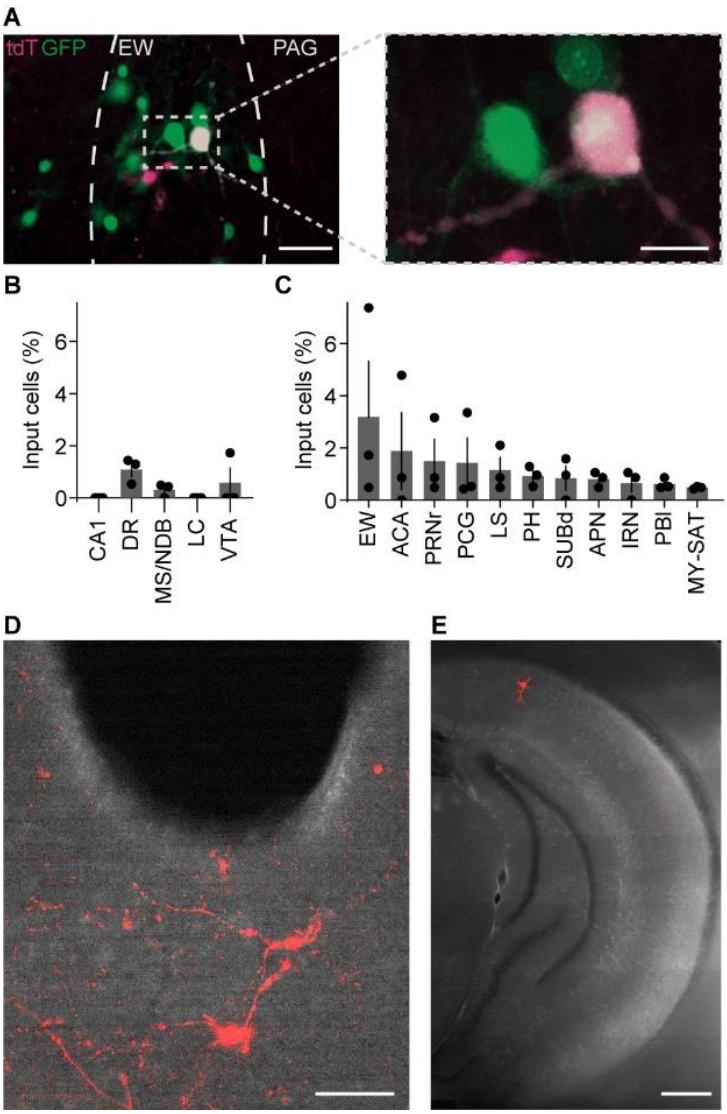

Figure S5. Monosynaptic retrograde tracing reveals a novel collection of inputs to the CART⁺ EW. Related to Figure 5.

(A) Fluorescence image (left; scale, 60 μm) of EW injected with CVS-N2c-ΔG-EnvA-tdT rabies virus (red) and CVS-N2c-ΔG-EnvA rabies virus helper viruses (green). Dashed gray box denotes inset shown in confocal image on right (scale, 20 μm). Individual starter cells can be seen.

(B) Monosynaptic retrograde labeling in brain regions previously proposed to project to the CART⁺ EW, as a percentage of total retrogradely labeled neurons (n = 3 mice). These areas show little to no evidence of monosynaptic retrograde labeling.

(C) As in (B), but brain regions with variable or sparse monosynaptic retrograde expression, as a percentage of total retrogradely labeled neurons (n=3 mice).

(D) Widefield image of immunoenhanced tdT⁺ cells (red) in the dorsal raphe. Scale, 100 μm.

(E) Similar to (E), but for the hippocampus. No retrogradely labeled neurons were observed in the hippocampus except for a sparse population in pyramidal neurons of the dorsal subiculum, i.e., SUBd in (C). Scale, 300 μm.

Error bars represent SEM.

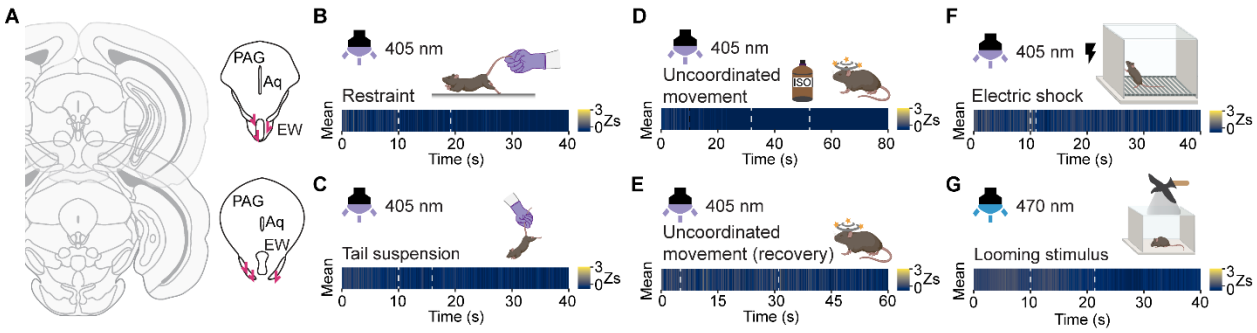

Figure S6. CART$^+$ EW GCaMP6s fluorescence signals are not motion artifacts. Related to Figure 6.

(A) Schematic of six representative fiber placements.

(B) Absence of time-locked fluorescence signals, displayed similarly to the time-locked fluorescence signals in the bottom panel of Figure 6C, in response to tail restraint (n = 6 mice, 1 trial) during excitation at the isosbestic point (purple light, 405 nm). Heatmap is identical to that used in Figures 6D, 6I, and 6J.

(C-F) As in (B), with isosbestic excitation, in response to (C) tail suspension (n = 6 mice, 3 trials), (D) uncoordinated movement following anesthetic exposure (n = 6 mice, 1 trial), (E) uncoordinated movement during recovery from anesthesia (n = 6 mice, 1 trial), and painful electric shock (n = 6 mice, 1 trial). Heatmap is identical to that used in (B) and Figures 6D, 6I, and 6J.

(G) As in (B), but with GCaMP fluorescent excitation with 470 nm light to reveal calcium concentration dependent fluorescent transients. A looming stimulus did not induce any fluorescent changes from the CART$^+$ EW (n = 6 mice, 6 to 7 trials each). Heatmap is identical to that used in (B) and Figures 6D, 6I, and 6J.

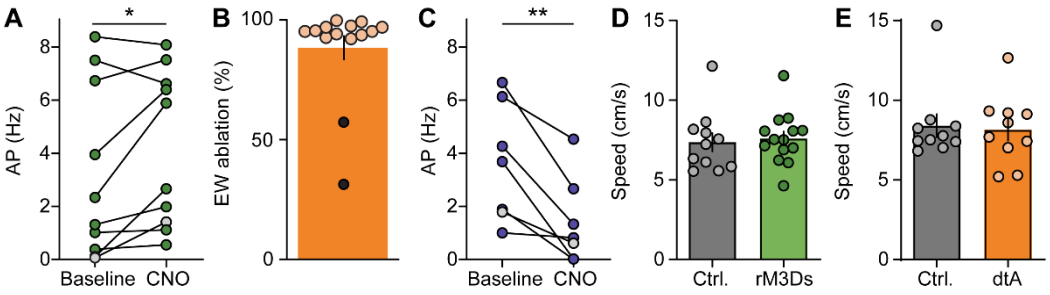

Figure S7. Validation of chemogenetic tools in CART$^+$ EW neurons. Related to Figure 7.

(A) Summary data of rM3Ds activation of CART$^+$ EW (n = 10 neurons, *p<0.05, paired t-test, $t_{(9)}$ = 2.333, p = 0.0445). The cell displayed in Figure 7E is marked (light gray).

(B) Example of quantification of EW ablation following dtA expression. Injection of dtA routinely killed >80% of neurons (orange). Mice with many EW cells remaining (black, n = 2)) were excluded from behavioral analysis.

(C) Summary data of hM4Di inactivation of CART$^+$ EW (n = 7 neurons, **p<0.01, paired t-test, $t_{(6)}$ = 4.204, p = 0.0057). The cell displayed in Figure 7F is marked (light gray).

(D) The average speed of mice in an open field does not differ between control and rM3Ds-expressing mice (unpaired t-test, $t_{(23)}$ = 0.3262, p = 0.7473, n = 11 Ctrl. mice, 14 rM3Ds mice).

(E) The average speed of mice in an open field does not differ between control and dtA-expressing mice (unpaired t-test, $t_{(18)}$ = 0.2493, p = 0.8059, n = 10 Ctrl. mice, 10 dtA mice).

Error bars represent SEM.